Mitochondrial fusion defects caused by CMT2A disease-associated variants of Mfn2

Samanas, N.B., Engelhart, E.A., Hoppins, S.

*Corresponding author:
Suzanne Hoppins
University of Washington
Department of Biochemistry
1959 NE Pacific Street
Health Sciences Building, J383
Seattle, WA 98195
Phone (206) 616 7565
Fax (206) 685 1792
e-mail: shoppins@uw.edu
ORCID – orcid/org/0000-0002-8070-3560

ABSTRACT

The peripheral neuropathy, Charcot Marie Tooth Syndrome Type 2A (CMT2A) is caused by amino acid substitutions in a component of the mitochondrial outer membrane fusion machine, mitofusin 2 (Mfn2). Mfn2 is predicted to exist in two conformational states, extended and closed; this would require that hinge regions mediate changes in the relative position of the two helical bundle domains (HB1 and HB2). Several disease-associated substitutions are located near the hinge that connects HB1 and HB2. We characterized these Mfn2 variants to assess the role of this domain in mitofusin-mediated fusion. While a fusion defect in cells was not evident, our cell-free mitochondrial fusion assay revealed a fusion deficit, which was compensated for by the addition of a cytosolic fraction. Consistent with this, all four variants had decreased nucleotide-dependent assembly. Given the partial loss of function associated with single substitution, we assessed fusion activity of variants with two substitutions in the hinge region. A variant with substitutions in both HB1 and HB2 was more severely impacted, with less fusion activity than a variant with two substitutions in HB1. These data support a model where conformational changes in Mfn2 require contribution from both helical bundle domains to support nucleotide-dependent assembly.

INTRODUCTION

Mitochondrial dynamics have become increasingly recognized as an important indicator of and contributor to both cellular health and death. Mitochondrial shape and cellular distribution change during the cell cycle, in response to stress, and as part of apoptosis (Scorrano 2013; Horbay & Bilyy 2016; Labbé et al. 2014; Tondera et al. 2009). Mitochondria are trafficked on microtubules and the overall shape and connectivity of the mitochondrial network is maintained or modified through mitochondrial fusion and division, which are mediated by membrane-remodeling large GTPase proteins of the dynamin related protein (DRP) family (Labbé et al. 2014). At steady state, it is estimated that mitochondrial fusion and division events are balanced. When mitochondrial division events exceed fusion events, the network fragments into many small individual mitochondria, and this fragmentation is associated with mitophagy and apoptosis. In contrast, when mitochondrial fusion occurs more frequently than division, the result is a more connected network comprised of longer mitochondria, which is associated with increased ATP production; i.e., during a cellular stress response. The importance of these processes and their regulation is highlighted by the association of dysregulated mitochondrial dynamics with various diseases such as Parkinson's disease, diabetes, and peripheral neuropathies (Züchner et al. 2004; Celardo et al. 2014; Vital & Vital 2012; Rovira-Llopis et al. 2017; Wada & Nakatsuka 2016).

Mitochondrial DRP-mediated fusion is poorly understood and is mechanistically distinct from both SNARE- and viral-mediated fusion. Fusion DRPs that reside in the outer and inner mitochondrial membranes are mitofusin 1, mitofusin 2 (Mfn1 and Mfn2) and Opa1, respectively. Mfn1 and Mfn2 are functionally related but non-redundant paralogs in mammalian cells (Santel & Fuller 2001; Eura 2003; Chen et al. 2003; Ishihara 2004). Interestingly, mutations in Mfn2, but not Mfn1, are the main cause of the peripheral neuropathy Charcot Marie Tooth Syndrome Type 2A (CMT2A) (Züchner et al. 2004). In CMT2A patients, distal nerve degeneration leads to weakness, sensory loss, gait impairment and foot deformations (Gemignani & Marbini 2001).

Fusion defects associated with some disease-associated variants of Mfn2 can be functionally complemented by Mfn1 (Detmer & Chan 2007b). Consistent with this, a recent report found that expression of exogenous Mfn1 in neurons of a CMT2A mouse model rescued axonal degradation (Zhou et al. 2019). The importance of the interaction between the mitofusin paralogs is further highlighted by the observation that the optimal fusion complex is composed of both Mfn1 and Mfn2 (Hoppins et al. 2011). As with other DRPs, both mitofusins exhibit nucleotide-dependent self-assembly, and the ability to form higher order oligomers has been correlated with fusion activity (Engelhart & Hoppins 2019). Further supporting a role for assembly in DRP-mediated fusion, intermolecular complementation has been observed between non-functional variants of the yeast mitofusin homolog Fzo1 that possess amino acid substitutions in distinct functional domains (Griffin & Chan 2006). Consistently, Fzo1 has been shown to form a large docking ring that generates an extensive area of contact at the interface of two mitochondria (Brandt et al. 2016).

Mitofusins contain four major structural domains including the GTPase domain, two sequential extended helical bundles (HB1 and HB2) connected by two short loops, and a transmembrane domain (Figure 1). The domain organization is similar to the bacterial DRP (BDLP), which has been structurally characterized (Low et al. 2009; Low & Löwe 2006). In BLDP, the relative positions of these domains changes in different nucleotide states via changes in hinge regions that connect the domains, resulting in either an extended or a closed state (Figure 1A and B). It is hypothesized that mitofusin proteins undergo similar structural rearrangements around hinge regions (Jimah & Hinshaw 2019). Indeed, atomic structures of a minimal GTPase domain construct of Mfn1 demonstrate that relative to the GTPase domain, HB1 can exist in two distinct, nucleotide-dependent conformations due to changes in Hinge 2 (Cao et al. 2017; Yan et al. 2018; Qi et al. 2016). Furthermore, mini-peptides or small molecules thought to alter the stability of the extended or closed state of mitofusin change the overall structure of the mitochondrial network in cells (Rocha et al. 2018; Franco et al. 2016).

There are over 100 unique amino acid substitutions associated with CMT2A, located in each of the functional domains of Mfn2 (Stuppia et al. 2015; Verhoeven et al. 2006). Interestingly, several disease-associated substitutions occur near Hinge 1, suggesting that this domain is

functionally important. To gain insight into the role of Hinge 1 in mitofusin-mediated membrane fusion, we interrogated the mitochondrial fusion activity and biochemical properties of disease-associated hinge variants. Our data indicate that this region is required for optimal mitochondrial fusion activity and efficient nucleotide-dependent assembly of Mfn2.

RESULTS

Mfn2 hinge variants restore reticular mitochondrial morphology in Mfn2-null cells

We set out to characterize four mutant variants of Mfn2 with amino acid substitutions within or adjacent to Loop 1 of Hinge 1: S378P, A383V, Q386P, and C390F (Figure 1C). While all cause CMT2A, S378P (Brockmann et al. 2008) and A383V (Muglia et al. 2009) have been reported in patients with less severe clinical phenotypes compared to patients with Q386P (Verhoeven et al. 2006) and C390F (Feely et al. 2011), who presented with very early age of onset (<2 years) and severe CMT phenotype (Table S1).

We began by analyzing mitochondrial morphology in stable cell lines expressing mutant versions of Mfn2. To create these lines, we introduced either wild type or mutant *MFN2* with a C-terminal 3xFLAG tag into Mfn2-null mouse embryonic fibroblasts (MEFs) using retroviral transduction (Chen et al. 2003). Clonal populations expressing Mfn2 at near-endogenous levels were selected for characterization (Figure S1).

In wild type MEFs, mitochondria were in reticular networks where most of the mitochondria were longer than 2.5μm (Figure 2, $Mfn1^{+/+}Mfn2^{+/+}$). Mfn2-null cells transduced with an empty vector, conversely, contained mainly fragmented individual mitochondria less than 2.5 μm in length (Figure 2, vector), which is consistent with published observations of Mfn2-null cells (Chen et al. 2003). Expression of wild type Mfn2 in Mfn2-null cells restored fusion activity and a reticular mitochondrial network in about 80% of cells (Figure 2, $Mfn2^{WT}$). Somewhat surprisingly, all Mfn2 mutant variants examined here ($Mfn2^{S378P}$, $Mfn2^{A383V}$, $Mfn2^{Q386P}$, and $Mfn2^{C390F}$) also restored a reticular mitochondrial network in Mfn2-null cells to a similar extent as $Mfn2^{WT}$. These results indicate that all four of these disease-causing substitutions in Mfn2 support fusion activity in Mfn2-null fibroblasts. This is consistent with previously reported data that showed subsets of CMT2A associated mutations restored fusion activity (Detmer & Chan

2007; Engelhart & Hoppins 2019). We reasoned that these substitutions may result in biochemical changes to the protein that were masked in the context of the cell, where many factors can modulate the structure of the mitochondrial network. Therefore, we proceeded to characterize these mutant forms of Mfn2 in the context of isolated mitochondria.

Mfn2 hinge variants have an in vitro mitochondrial fusion defect

To quantify the mitochondrial fusion activity of the Mfn2 mutant variants in the absence of cytosolic factors, we utilized a cell-free mitochondrial fusion assay. Mitochondria isolated from cells expressing RFP or CFP targeted to the mitochondrial matrix were mixed, incubated in fusion buffer and then imaged by fluorescence microscopy. Fusion events were scored as the overlap of the two fluorophores in three dimensions. All assays were performed in parallel with mitochondria isolated from wild type cells, and data is expressed as a proportion of WT. Mitochondria isolated from Mfn2-null cells transduced with empty vector fused at a much lower frequency than wild type controls (Figure 3A). Fusion of mitochondria isolated from the clonal population of Mfn2-null cells expressing $Mfn2^{WT}$ was similar to wild type controls (Figure 3A), consistent with the restoration of the mitochondrial morphology in cells. To quantify the fusion activity of the Mfn2 hinge mutants in vitro, mitochondria were isolated from each of the clonal populations described above. In each case, the mitochondrial fusion activity was significantly lower than wild type controls (Figure 3A).

The in vitro mitochondrial fusion data revealed that amino acid substitutions in this hinge region diminish the fusion capability of Mfn2. Given that we could not detect a mitochondrial fusion defect in cells, we predicted that a cytosolic factor could be enhancing fusion activity of the mutant variants. To test this in vitro, we performed the mitochondrial fusion assay in the presence of a cytosol-enriched fraction from wild type MEFs. As has been previously reported, the addition of the cytosol-enriched fraction to wild type mitochondria moderately stimulated fusion activity (Hoppins et al. 2011). In contrast, the cytosol-enriched fraction did not alter the fusion activity of mitochondria isolated from Mfn2-null cells, indicating that Mfn2, but not Mfn1, is regulated by the cytosolic factor (Figure 3B). The addition of cytosol also increased the fusion activity of mitochondria that possess the Mfn2 hinge variants similarly to wild type

controls (Figure 3B). These data indicate that the fusion defect associated with the hinge mutant variants can be compensated for by cytosolic factors in cells.

Mfn2 hinge mutant variants interact with Mfn1 in cis and in trans

Mfn1 and Mfn2 physically interact in the same membrane, in cis, and across two membranes, in trans, as measured by co-immunoprecipitation (Engelhart & Hoppins 2019; S. A. Detmer & Chan 2007a; Chen et al. 2003). To determine if the Mfn2 hinge mutant variants interact with Mfn1 in cis or in trans, we tested whether Mfn1 would co-immunoprecipitate with Mfn2-FLAG. To distinguish between cis and trans, we mixed mitochondria that possess endogenous Mfn1 and Mfn2-FLAG with mitochondria that possess Mfn1-EGFP and endogenous Mfn2 (Figure 4A). In this way, three unique interactions with Mfn2-FLAG (Figure 4, filled arrowhead) could be assessed: (1) endogenous Mfn1 in cis (Figure 4, black arrow), (2) Mfn1-EGFP in trans (Figure 4, open arrowhead), and (3) endogenous Mfn2 in trans (Figure 4, white arrow). These reactions were performed in the presence of the GTP transition state mimic GDP-BeF_3, which has been shown to stabilize an interaction between mitofusin molecules and promote a tethering interaction, or BeF_3 alone as a negative control (Yan et al. 2018; Qi et al. 2016). As expected, wild type Mfn2-FLAG immunoprecipitated both endogenous Mfn1 and Mfn1-EGFP (Figure 4). The amount of endogenous Mfn1 interacting in cis (Figure 4, black arrow) is not significantly different in the presence or absence of the transition state mimic. In contrast, the trans interaction is more robust in the presence of GDP-BeF_3 compared to BeF_3 alone (Figure 4, open arrowhead). Together, these data indicate that only the trans interaction is highly dependent on the nucleotide binding state of the mitofusin proteins. Each of the four Mfn2 hinge variants also immunoprecipitated Mfn1 in cis and in trans (Figure 4), indicating that there is no defect in the physical interaction with Mfn1 in either context. Interestingly, even in the presence of GDP-BeF_3, we could not detect an interaction in trans between Mfn2-FLAG and endogenous Mfn2 (Figure 4, white arrow), which suggests that Mfn2 does not form a robust homotypic trans complex.

Nucleotide-dependent self-assembly is diminished in Mfn2 hinge mutant variants

Defects in mitofusin assembly correlate with reduced rates of mitochondrial fusion in vitro (Engelhart & Hoppins 2019). To determine the capacity of the Mfn2 hinge variants to

assemble, we utilized blue native gel electrophoresis (BN-PAGE). Mitochondria were left untreated or incubated with either GTP or the non-hydrolyzable analog GMPPNP. Mitochondria were then lysed and separated by BN-PAGE and subject to Western blot analysis. When mitochondria were left untreated, $Mfn2^{WT}$ migrated mostly in assemblies that approximately correspond in size to a dimer (Figure 5, arrow), with some protein migrating as larger assemblies (Figure 5, arrowheads). When these mitochondria were instead incubated with nucleotide, the ratio of dimer to larger assemblies decreased, consistent with nucleotide-dependent assembly of Mfn2 into higher-order oligomers. Specifically, following incubation with GTP, more $Mfn2^{WT}$ migrated in two larger assemblies, with a notable increase in the oligomer that corresponds approximately in size to a tetramer (Figure 5, open arrowhead). Incubation of mitochondria with GMPPNP also promoted higher-order assembly with enhanced stability of a predicted trimer and some protein migrating as a predicted tetramer (Figure 5, closed and open arrowheads, respectively). Together, these data indicate that Mfn2 exists primarily as a dimer in the mitochondrial outer membrane and assembles into a trimer and tetramer in a nucleotide-dependent manner.

In the absence of nucleotide all of the Mfn2 hinge mutants migrated similarly to wild type, with most of the protein in the dimer (Figure 5). In the presence of GTP, the mutants also assembled similar to wild type, with the exception of $Mfn2^{S378P}$, which had less protein migrating as a tetramer compared to wild type. Each of the hinge mutants displayed altered assembly relative to wild type Mfn2 in the presence of GMPPNP (Figure 5B). Compared to $Mfn2^{WT}$, $Mfn2^{S378P}$, $Mfn2^{A383V}$, $Mfn2^{Q386P}$, and $Mfn2^{C390F}$ all showed a significantly decreased shift in the amount of protein migrating as a timer (Figure 5B). These data indicate that amino acid substitutions in this hinge region prevent the stable assembly of Mfn2 into the predicted trimer in the presence of the non-hydrolyzable GTP analog. Given that these mutant variants also exhibit an in vitro mitochondrial fusion defect, we hypothesize that nucleotide dependent assembly contributes to efficient Mfn2-mediated membrane fusion.

Double hinge mutations reveal that HB1 and HB2 work together in mitochondrial fusion

Our data indicate that the hinge connecting HB1 and HB2 is important for Mfn2 fusion activity, but the biochemical defects associated with each of the mutants are modest. Therefore, we

considered the possibility that HB1 and HB2 both contribute to conformational changes at the hinge. If this is the case, amino acid substitutions in both HB1 and HB2 together should be more severe than either single change. To test this hypothesis, we used Mfn2^{L710P}, a disease-associated variant in HB2 that is located near Loop 2 in Hinge 1 (Verhoeven et al. 2006) (Figure 1, Figure S2). This amino acid substitution has been characterized in Mfn1, Mfn1^{L691P}, which had some fusion activity in Mfn1-null cells (Koshiba et al. 2004). We generated double mutant variants of Mfn2 with this mutation and either Mfn2^{S378P}, which is located in HB1 or Mfn2^{C390F}, which is located in HB2 (Mfn2$^{S378P/L710P}$ and Mfn2$^{C390F/L710P}$, respectively).

To determine the fusion activity of these double mutant variants, we utilized retroviral transduction to express Mfn2-mNeonGreen (Mfn2-NG) in Mfn2-null MEFs which has previously been shown to restore fusion activity (Engelhart & Hoppins 2019). The mitochondrial morphology was scored in cells expressing Mfn2, as assessed by colocalization of Mfn2-NG with MitoTracker Red. As expected, Mfn2^{WT}, Mfn2^{S378P} and Mfn2^{C390F} restored the reticular mitochondrial network, which recapitulated our observations from the clonal populations described above (Figure 6, compare to Figure 2). Expression of Mfn2^{L710P} also restored a reticular network in 65% of cells (Figure 6), indicating a mild defect in mitochondrial fusion, consistent with previous reports (Koshiba et al. 2004).

In Mfn2-null cells expressing the HB2 double mutant Mfn2 $^{C390F/L710P}$, the mitochondrial morphology was comparable to that in cells expressing Mfn2^{L710P} alone (Figure 6). In contrast, when both HB1 and HB2 possess an amino acid substitution, there is significantly less mitochondrial fusion. Specifically, in Mfn2-null cells expressing Mfn2 $^{S378P/L710P}$, most cells possessed a mitochondrial network that was either fragmented or in fragmented aggregates, and only 30% of cells had a reticular mitochondrial network. Together, these results support the conclusion that HB1 and HB2 work together to support Mfn2-mediated membrane fusion.

DISCUSSION

In this study, we performed an in-depth characterization of disease-associated amino acid substitutions located within Hinge 1 of Mfn2, which connects HB1 and HB2. In other DRPs,

hinges mediate conformational changes that are required for membrane remodeling function. The results presented here are consistent with structural models that suggest that this region functions as a hinge and for the first time connects Hinge 1 function to nucleotide-dependent assembly of the mitofusins. These molecular defects also correspond to a decrease in mitochondrial fusion efficiency in vitro, which can be compensated for by cytosolic factors both in cells and in a cell-free mitochondrial fusion assay.

Our analysis of Mfn2 assembly by BN-PAGE indicates that the nucleotide binding state of the protein influences the assembly state. Our data indicate that most Mfn2 exists as a dimer in the mitochondrial outer membrane and that GTP stabilizes a predicted tetramer while the non-hydrolyzable analog stabilizes a predicted trimer. In the presence of GTP, most of the hinge mutants are very similar to wild type and can form dimers and tetramers. This indicates that these variants are not unable to fold or oligomerize. In contrast, the hinge mutants do not readily form the trimeric state adopted when Mfn2 is bound to GMPPNP. Given that all Mfn2 hinge mutants co-immunoprecipitate Mfn1 as efficiently as wild type, the interaction with Mfn1 is not likely to play a role in assembly as a trimer. Indeed, previously published data from our lab indicate that the BN-PAGE assemblies are homo-oligomers (Engelhart & Hoppins 2019). These data are consistent with the hypothesis that the nucleotide binding state of Mfn2 alters the conformational state of the protein which results in the preferential formation of a dimer, trimer, or tetramer. Therefore, the reduced assembly of the trimer by the hinge mutants could be due to aberrant structural rearrangements of HB1 and HB2 as mediated by Hinge 1.

Intermolecular functional complementation between mitofusin molecules has been observed previously. Disease-associated variants of Mfn2 that do not support fusion alone are able to contribute to fusion activity when Mfn1 is also present (Detmer & Chan 2007a). In yeast, co-expression of two non-functional variants of Fzo1 also results in functional complementation (Griffin & Chan 2006). These data indicate that different molecules in the fusion complex can contribute different properties. Here we present evidence that different structural domains in a single molecule also work together. When two disease-associated amino acid substitutions are located in the same helical bundle, the fusion activity of Mfn2 is comparable to a single mutant variant. In contrast, one substitution in each HB1 and HB2 results in a significant decrease in

fusion activity. These data support the hypothesis that Mfn2 contains at least one functionally important hinge that facilitates structural rearrangement during mitochondrial fusion.

As a whole, the data presented here are consistent with the hypothesis that different nucleotide-dependent conformations support either the formation or stabilization of different assembly states and that the hinge that connects HB1 and HB2 plays a role in this process.

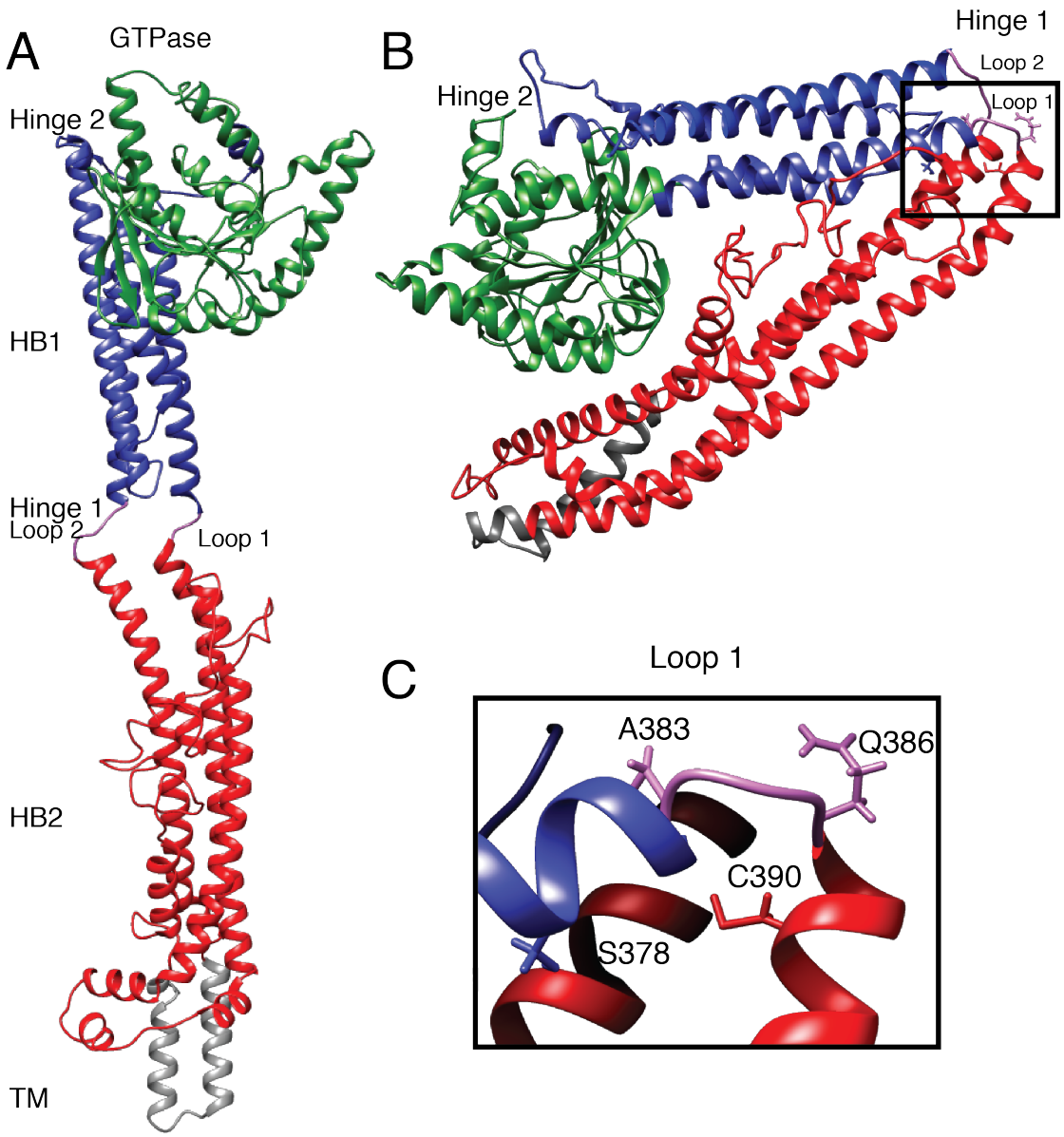

Figure 1. Structural model of the positions of Hinge 1 amino acid substitutions associated with CMT2A.

(A) Structural model of the predicted extended structure of Mfn2 based on the crystal structure of the structurally related protein BDLP with GMPPNP (PDB 2W6D). The GTPase domain is green, HB1 is blue, HB2 is red, the transmembrane (TM) domain is grey, and Loops 1/ 2 are purple. Structural prediction performed by I-TASSER server (Yang & Zhang 2015; Zhang 2009). **(B)** Structural model of the predicted closed structure of Mfn2 based on the crystal structure of the structurally related protein BDLP with GDP (PDB 2J69). Domains are colored as described in (A). Structural prediction performed by I-TASSER server (Yang & Zhang 2015; Zhang 2009). **(C)** Enlarged view of Loop 1 from Hinge 1 showing the positions of the CMT2A-related amino acids.

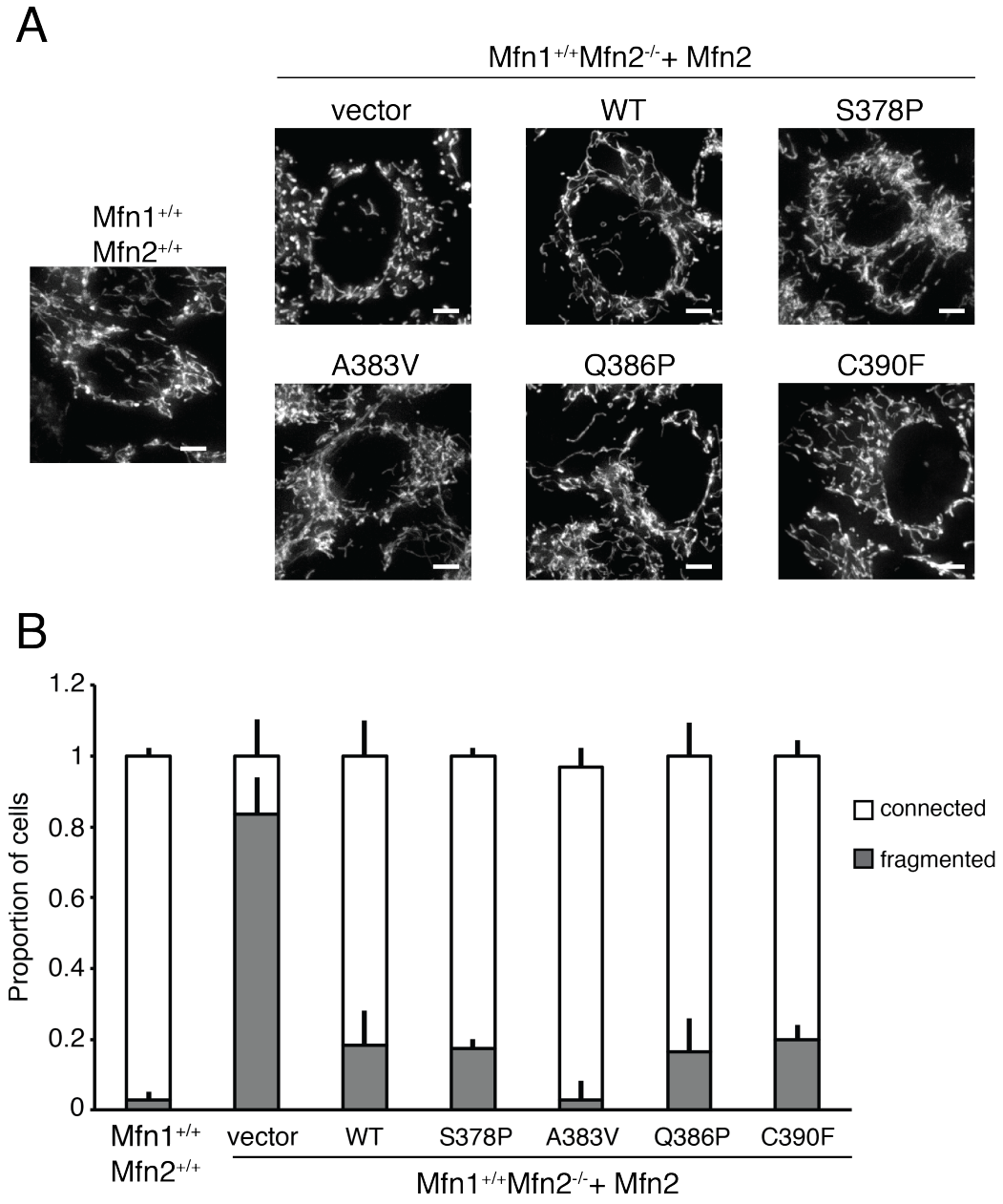

Figure 2. Mfn2 hinge variants support mitochondrial fusion when expressed in Mfn2-null cells. (A) Representative images of mitochondrial networks in wild type ($Mfn1^{+/+}Mfn2^{+/+}$) or Mfn2-null ($Mfn1^{+/+}Mfn2^{-/-}$) mouse embryonic fibroblasts expressing the indicated Mfn2 variant. Mitochondria were stained with Mitotracker Red CMXRos and visualized by fluorescence microscopy. Images represent a maximum intensity projection. Scale bars = 5 μm. **(B)** Quantification of mitochondrial morphology in cells represented in **(A)** Error bars indicate mean + standard deviation from three blinded experiments ($n \geqq 100$ cells per population per experiment).

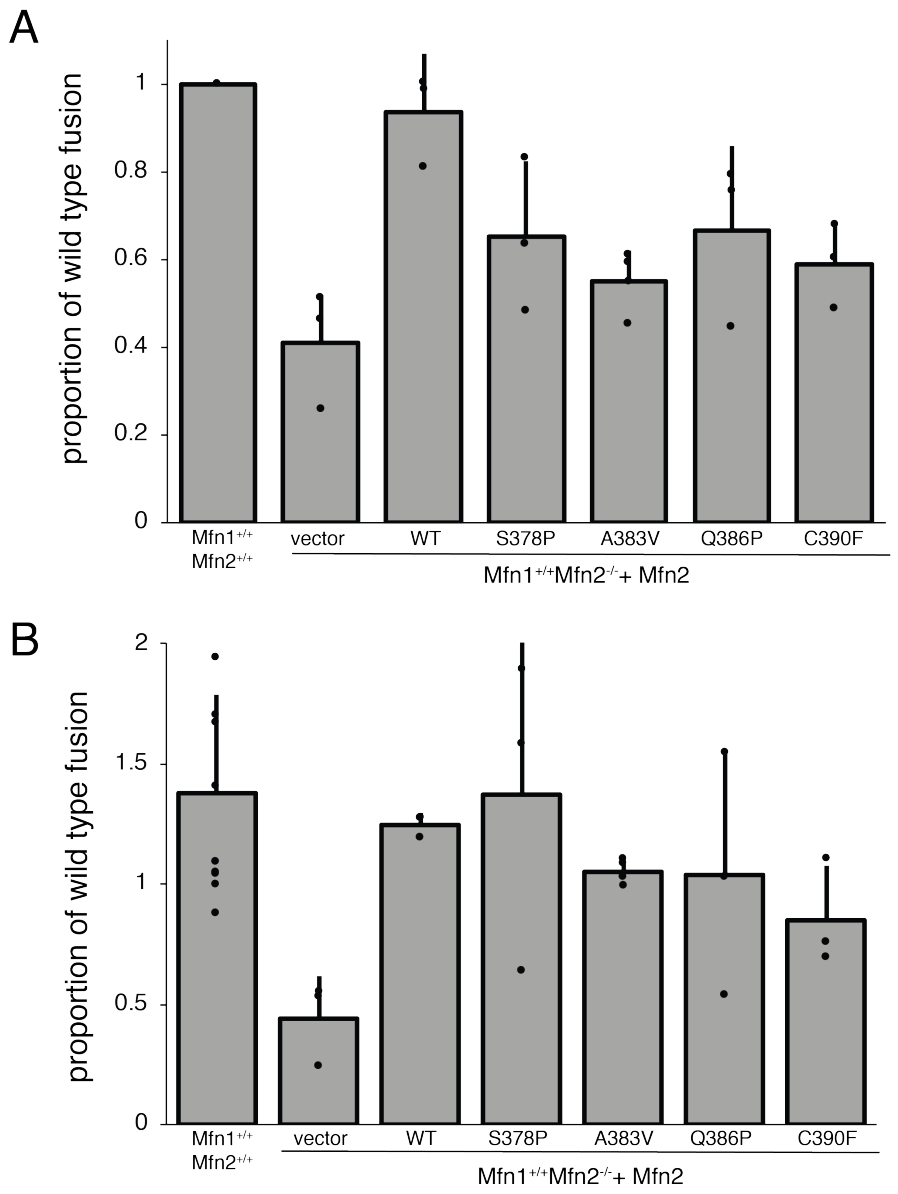

Figure 3. Mitochondrial in vitro fusion assay reveals a defect for all Mfn2 hinge variants. **(A)** Mitochondria were isolated from wild type cells or clonal populations of Mfn2-null cells either transduced with empty vector or expressing the indicated Mfn2 variant were subject to in vitro fusion conditions at 37°C for 60 minutes. The data are represented as relative to wild type controls performed in parallel. Error bars indicate mean + standard deviation from at least three independent experiments and the statistical significance were determined by paired t-test analysis (*P<0.05). **(B)** Mitochondrial in vitro fusion assay performed as in (A) except with the addition of cytosol-enriched fraction to the reaction buffer. Data are represented as relative to wild type controls performed in parallel without cytosol added. Error bars indicate mean + standard deviation from at least three independent experiments

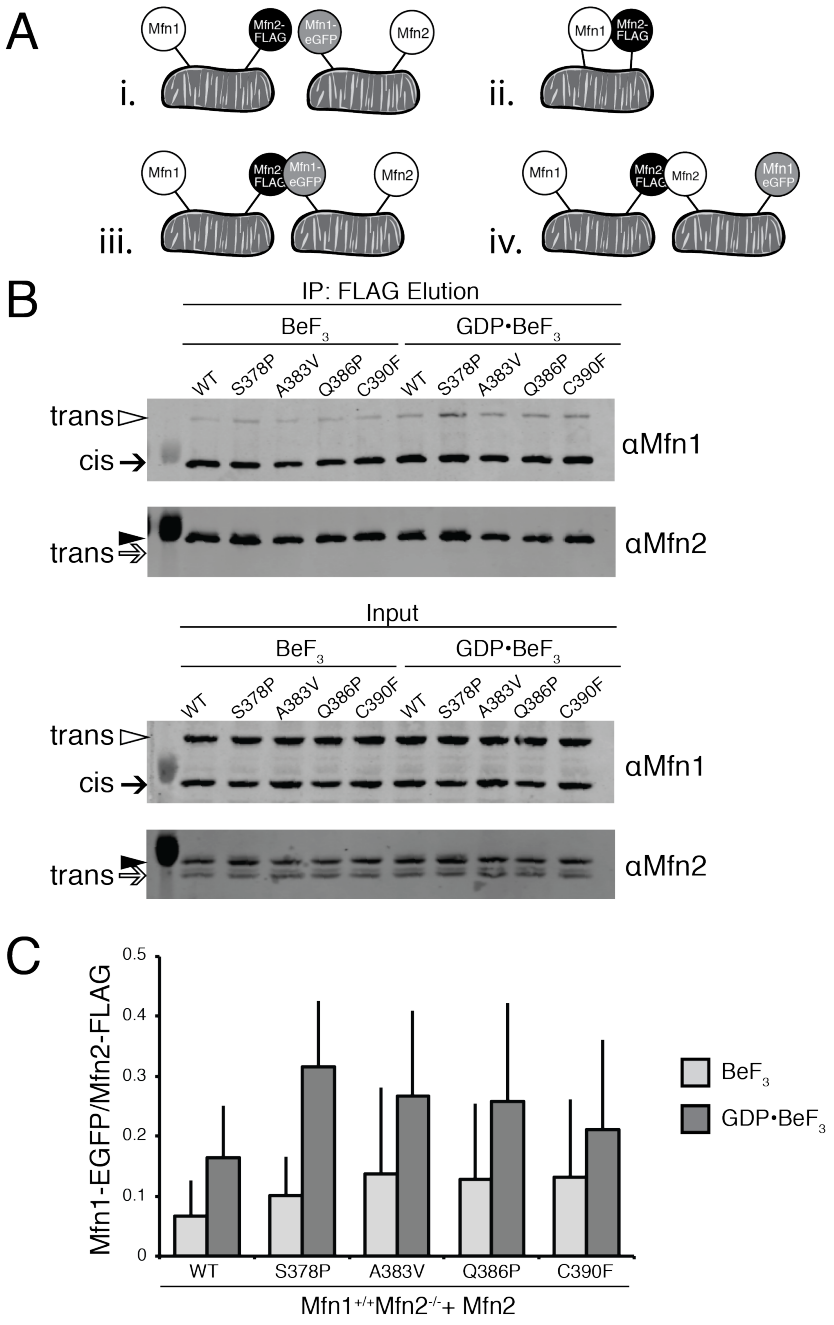

Figure 4. Mfn2 hinge variants interact with Mfn1 in cis and trans.

(A) Schematic of the differential epitope labeling utilized in the co-immunoprecipitation assay. **(B)** Mitochondria were isolated from a clonal population of Mfn1-null cells expressing $Mfn1^{WT}$-EGFP at endogenous levels ($Mfn1^{WT}Mfn2^{+/+}$), and clonal populations of Mfn2-null cells expressing the indicated Mfn2-FLAG variants. Mitochondria that possess Mfn1-EGFP and Mfn2 were combined with mitochondria that possess Mfn1 and Mfn2-FLAG and these mixtures were incubated with BeF_3 in the absence or presence of GDP. Following lysis, immunoprecipitation was performed with α-FLAG

magnetic beads. Proteins eluted from the beads were subjected to SDS-PAGE and immunoblotting with α-Mfn1 and α-Mfn2, as indicated. Arrows indicate endogenous Mfn1 (black) and Mfn2 (white); arrowheads indicate Mfn1-EGFP (white) and Mfn2-FLAG (black), respectively. Input represents 3% of the input and elution represents 37.5% of the immunoprecipitated protein. **(C)** Quantification of the percentage of Mfn1-EGFP in the elution compared to Mfn2-FLAG is shown as the mean + standard deviation of three independent experiments.

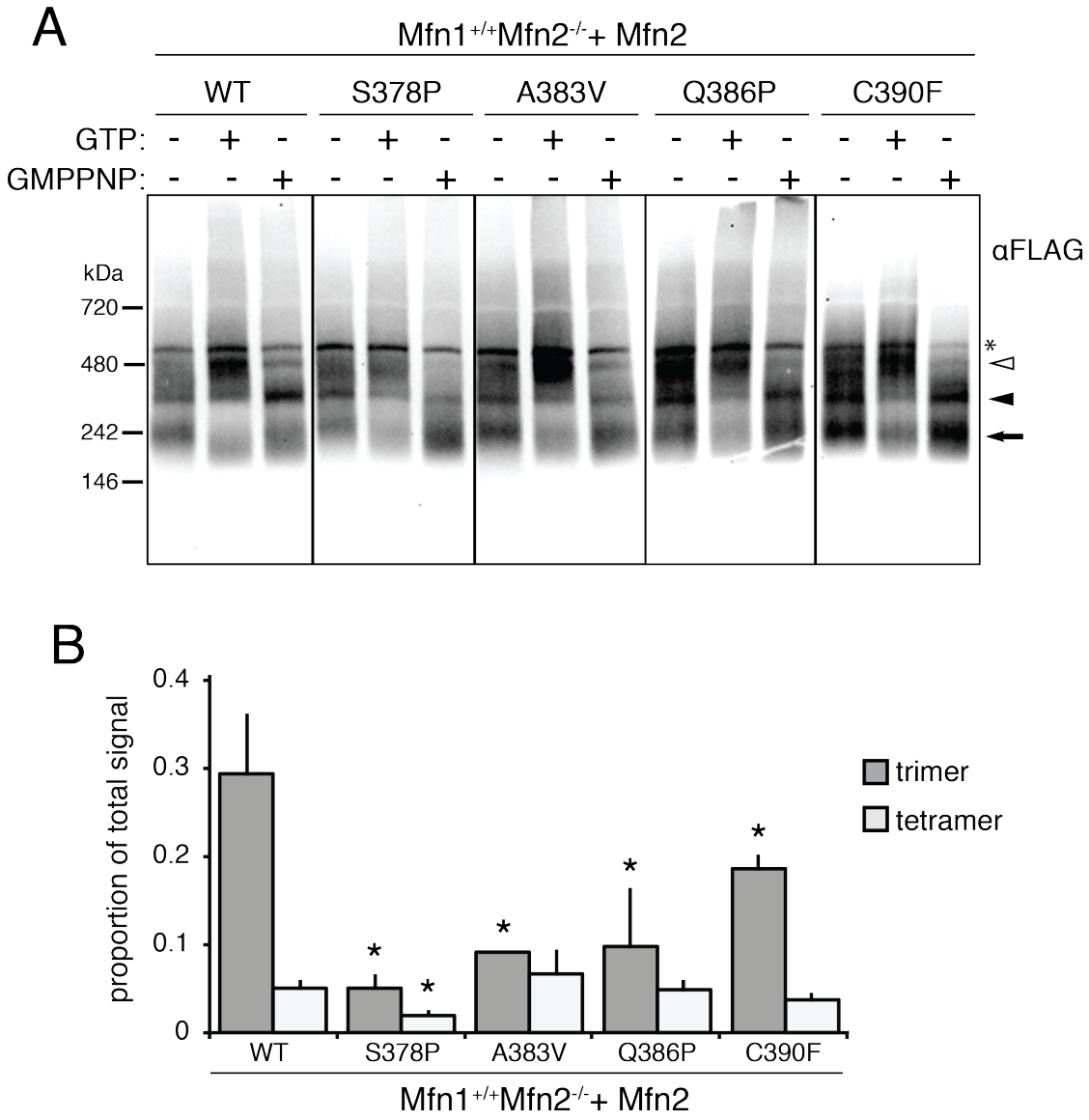

Figure 5. Mfn2 hinge variants have altered nucleotide-dependent assembly.

(A) Mitochondria were isolated from clonal populations of Mfn2-null cells expressing the indicated Mfn2 variant. Mitochondria were either untreated or incubated with 2mM GTP or 2mM GMPPNP as indicated before lysis and separation by BN-PAGE followed by immunoblotting with anti-FLAG antibody. Arrow represents dimer, closed arrowhead indicates trimer, and open arrowhead indicates tetramer. Asterisk (*) indicates nonspecific signal. **(B)** Quantification of proportion of the total protein that is running in the trimer or tetramer band after treatment with GMPPNP (filled arrowhead). Error bars indicate mean + standard deviation from at least three independent experiments and the statistical significance were determined by paired t-test analysis between the indicated data and wild type (*P<0.05).

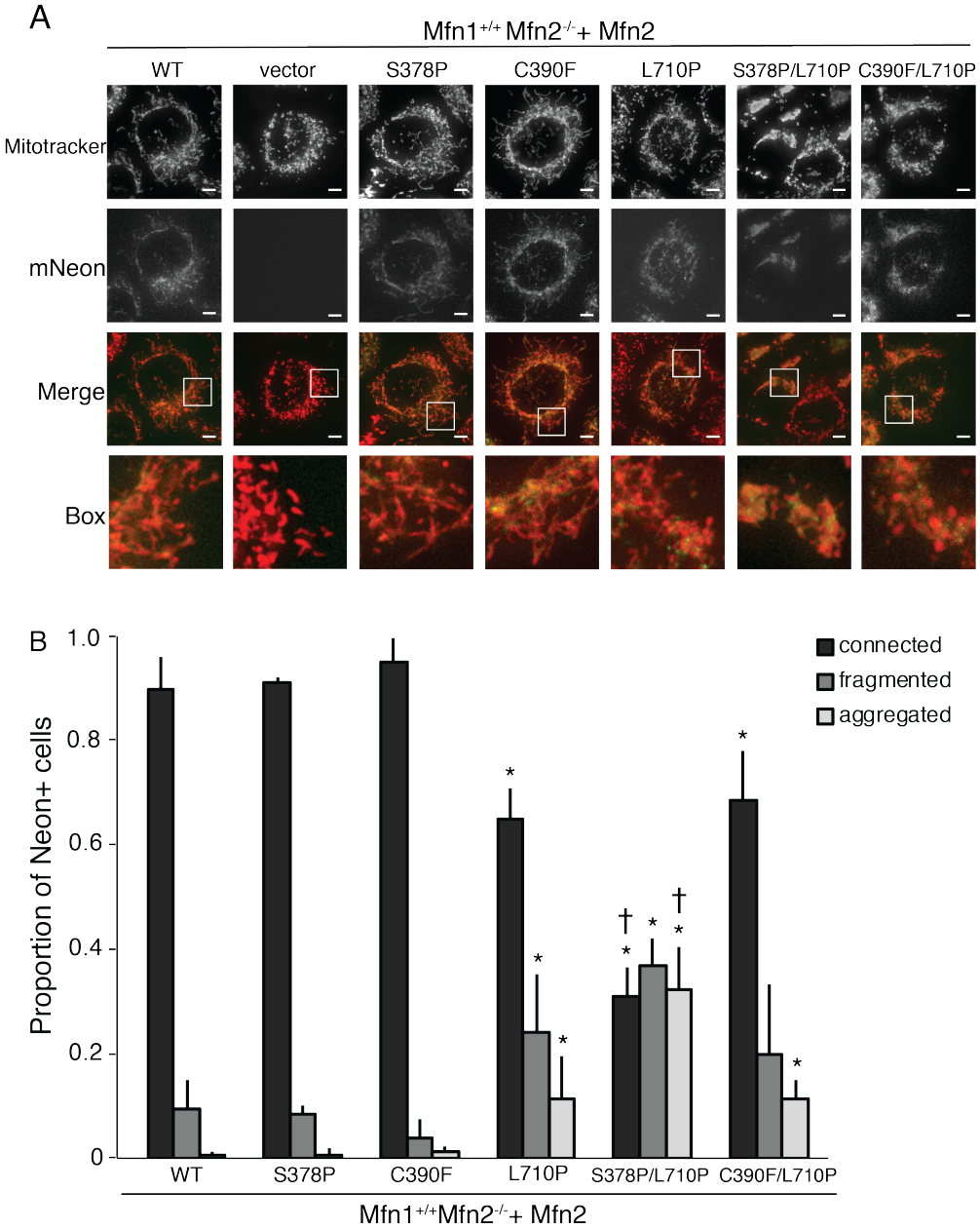

Figure 6. Mfn2 variants with substitutions in both HB1 and HB2 are defective for fusion in Mfn2-null cells.

(A) Representative images of mitochondrial networks in Mfn2-null ($Mfn1^{+/+}Mfn2^{-/-}$) mouse embryonic fibroblasts expressing the indicated Mfn2-mNeonGreen variant. Mitochondria were stained with Mitotracker Red CMXRos and visualized by fluorescence microscopy. Images represent a maximum intensity projection. Scale bars = 5 μm. **(B)** Quantification of mitochondrial morphology of cells represented in **(A).** Error bars indicate mean + standard deviation from at least three independent experiments and the statistical significance were determined by paired t-test analysis between the indicated data and wild type (*P<0.05) or between the indicated data and $Mfn2^{S378P/L710P}$ (†P<0.05).

MATERIALS AND METHODS

Cell culture

All cells were grown at 37°C and 5% CO_2 and cultured in DMEM (Thermo Fisher Scientific) containing 1X GlutaMAX (Thermo Fisher Scientific) with 10% FBS (Seradigm) and 1% penicillin/streptomycin (Thermo Fisher Scientific). Mouse embryonic fibroblasts cells (Mfn wildtype and Mfn2-null) were purchased from ATCC.

Retroviral transduction and generation of clonal populations

Plat-E cells (Cell Biolabs) were maintained in complete media supplemented with 1 μg/mL puromycin and 10 μg/mL blasticidin and plated at approximately 80% confluency the day prior to transfection. Plat-E cells were transfected with FuGENE™ HD (Promega) and transfection regent was incubated overnight before a media change. Viral supernatants were collected at approximately 48, 56, 72, and 80 hours post transfection and incubated with MEFs in the presence of 8 mg/ml polybrene. Approximately 16 hours after the last viral transduction, MEF cells were split and selection was added if needed (1 μg/mL puromycin or 200 μg/mL hygromycin).

Clonal populations were generated by plating cells at very low density and clones were collected onto sterile filter paper dots soaked in trypsin. Following expansion, whole cell extract from clonal populations were screened by western blot analysis for mitofusin against wildtype controls.

Transfection and microscopy

All cells were plated in No. 1.5 glass-bottomed dishes (MatTek). Mouse embryonic fibroblasts were incubated with 0.1 μg/mL Mitotracker Red CMX Ros (Invitrogen) for 15 minutes at 37°C with 5% CO_2, washed and incubated with complete media for at least 45 minutes prior to imaging. MEFs were imaged at 37°C with 5% CO_2. A Z-series with a step size of 0.3 μm was collected with a Nikon Ti-E widefield microscope with a 63X NA 1.4 oil objective (Nikon), a solid-state light source (Spectra X, Lumencor), and an sCMOS camera (Zyla 5.5 Megapixel). Each cell line was imaged by a blinded researcher on at least three separate occasions (n > 100 cells per experiment).

Image analysis

Images were deconvolved using 8-15 iterations of 3D Landweber deconvolution. Deconvolved images were then analyzed using Nikon Elements software. Maximum intensity projections were created using Photoshop (Adobe). Mitochondrial morphology was scored as follows: reticular indicates that fewer than 30% of the mitochondria in the cell were fragments (fragments defined as mitochondria less than 2 μm in length); fragmented indicates that most of the mitochondria in the cell were less than 2 μm in length; aggregated indicates fragmented mitochondria that were not distributed throughout the cytosol.

Preparation of mitochondria or cytosol-enriched fraction

For each experiment, three to five 15 cm plates each of MEFs were grown to ~90% confluency. Cells were harvested by cell scrapping, pelleted, and washed in mitochondrial isolation buffer (MIB) (0.2 M sucrose, 10 mM Tris-MOPS [pH 7.4], 1 mM EGTA). The cell pellet was resuspended in one cell pellet volume of cold MIB, and cells were homogenized by 10 to 14 strokes on ice with a Kontes Potter-Elvehjem tissue grinder set at 400 RPM. The homogenate was centrifuged (500 × *g*, 5 min, 4°C) to remove nuclei and unbroken cells, and homogenization of the pellet fraction was repeated followed by centrifugation at 500 × *g*, 5 min, 4°C. The supernatant fractions were combined and centrifuged again at 500 × *g*, 5 min, 4°C to remove remaining debris. The supernatant was transferred to a clean microfuge tube and centrifuged (7400 × *g*, 10 min, 4°C) to pellet a crude mitochondrial fraction. The post-mitochondrial supernatant fraction was saved as the cytosol-enriched fraction. The crude mitochondrial pellet was resuspended in a small volume of MIB. Protein concentration of fractions was determined by Bradford assay (Bio-Rad Laboratories).

In vitro mitochondrial fusion

An equivalent mass (12.5 μg) of mtTagRFP and mtCFP mitochondria were mixed, washed in 500uL MIB and concentrated by centrifugation (7400 × *g*, 10 min, 4°C). Following a 10 min incubation on ice, the supernatant was removed and the mitochondrial pellet was resuspended in 10 μl fusion buffer (20 mM PIPES-KOH [pH 6.8], 150 mM KOAc, 5 mM $Mg(OAc)_2$, 0.4 M sorbitol, 0.12 mg/ml creatine phosphokinase, 40 mM creatine phosphate, 1.5 mM ATP, 1.5 mM

GTP) or 10 μl cytosol-enriched buffer (2.5 μL of the cytosol-enriched fraction obtained from WT MEFs and 7.5 μL fusion buffer). Fusion reactions were incubated at 37°C for 60 minutes.

Analysis of mitochondrial fusion

Mitochondria were imaged on depression microscope slides by pipetting 4μL fusion reaction onto a 3% low-melt agarose bed, made in modified fusion buffer (20 mM PIPES-KOH [pH 6.8], 150 mM KOAc, 5 mM $Mg(OAc)_2$, 0.4 M sorbitol). A Z-series of 6 0.2 μm steps was collected with a Nikon Ti-E widefield microscope with a 100X NA 1.4 oil objective (Nikon), a solid state light source (Spectra X, Lumencor), and a sCMOS camera (Zyla 5.5 Megapixel). For each condition tested, mitochondrial fusion was assessed by counting ≥ 300 total mitochondria per condition from ≥ 4 images per condition (50 – 200 mitochondria per image collected), and fusion was scored by colocalization of the red and cyan fluorophores in three dimensions.

BN-PAGE

Isolated mitochondria (15 – 30 μg) were incubated with or without 2 mM nucleotide and 2.5 mM $BeSO_4$, and 25 mM NaF as indicated in 0.2 M sucrose, 10 mM Tris-MOPS [pH 7.4], 1 mM EGTA, 5 mM $Mg(OAc)_2$ buffer at 37°C for 30 minutes. Mitochondria were then lysed in 1% w/v digitonin, 50 mM Bis-Tris, 50 mM NaCl, 10% w/v glycerol, 0.001% Ponceau S; pH 7.2 for 15 minutes on ice. Lysates were centrifuged at 16,000 x *g* at 4° C for 30 minutes. The cleared lysate was mixed with Invitrogen NativePAGE™ 5% G-250 Sample Additive to a final concentration of 0.25%. Samples were separated on a Novex™ NativePAGE™ 4 - 16% Bis-Tris Protein Gels (Invitrogen) at 4°C. Gels were run at 40 V for 30 minutes then 100 V for 30 minutes with dark cathode buffer (1X NativePAGE™ Running Buffer (Invitrogen), 0.02% (w/v) Coomassie G-250). Dark cathode buffer was replaced with light cathode buffer (1X NativePAGE™ Running Buffer (Invitrogen), 0.002% (w/v) Coomassie G-250) and the gel was run at 100 V for 30 minutes and subsequently at 250 V for 60-75 minutes until the dye front ran off the gel. After electrophoresis was complete, gels were transferred to PVDF membrane (Bio-Rad Laboratories) at 30 volts for 16 hours in transfer buffer (25 mM Tris, 192 mM glycine, 20% methanol). Membranes were incubated with 8% acetic acid for 15 minutes and washed with H_2O for 5 minutes. Membranes were dried at 37°C for 20 minutes and then rehydrated in

100% methanol and washed in H_2O. Membranes were blocked in 4% milk for 20 minutes and were probed with anti-FLAG (Sigma) for 4 hours at room temperature or overnight at 4°C. Membranes were incubated with HRP-linked secondary antibody (Cell Signaling Technology) at room temperature for 1 hour. Membranes were developed in SuperSignal Femto ECL reagent (Thermo Fisher Scientific) for 5 minutes and imaged on iBright Imaging System (Thermo Fisher Scientific). Band intensities were quantified using ImageJ software (NIH). NativeMark Unstained Protein Standard (Life Technologies) was used to estimate molecular weights of mitofusin protein complexes.

Co-immunoprecipitation

Differentially tagged isolated mitochondrial populations (50 μg each) were mixed together. Mitochondria were incubated at 37°C for 30 minutes with beryllium fluoride (2.5 mM $BeSO_4$, 25 mM NaF) with or without 2 mM GDP in fusion buffer (20 mM PIPES-KOH [pH 6.8], 150 mM KOAc, 5 mM $Mg(OAc)_2$, 0.4 M sortibal with 0.12 mg/mL creatine kinase, 40 mM creatine phosphate, 1.5 mM ATP). Mitochondria were solubilized in lysis buffer (20 mM HEPES-KOH [pH 7.4], 50 mM KCl, 5 mM $MgCl_2$) with 1.5% w/v n-Dodecyl β-D-maltoside (DDM), and 1X Halt Protease Inhibitor (Thermo Scientific) for 30 minutes on ice. Lysates were cleared at 10,000 x *g* for 15 minutes at 4°C. Supernatant was incubated with 50 mL magnetic μMACS Anti-DYKDDDDK MicroBeads (Miltenyi Biotec) for 30 minutes on ice. The sample was applied to a MACS Column (Miltenyi Biotec) placed in the magnetic field using a μMACS Separator (Miltenyi Biotec) and washed once with 300 mL 20 mM HEPES-KOH [pH 7.4], 50 mM KCl, 5 mM $MgCl_2$, 0.1% DDM and once with 200 mL 20 mM HEPES-KOH [pH 7.4], 50 mM KCl, 5 mM $MgCl_2$. One column volume (25 ml) SDS-PAGE loading buffer (60 mM Tris-HCl [pH 6.8], 2.5% sodium dodecyl sulfate, 5% βME, 5% sucrose, 0.1% bromophenol blue) was incubated for 15 minutes at room temperature and proteins were eluted once with 40 mL SDS-PAGE loading buffer. Samples were run on an SDS-PAGE gel and transferred onto nitrocellulose at 94V for 1 hour in 1X transfer buffer (25 mM Tris, 192 mM glycine, 20% methanol). Membranes were blocked in 4% Milk for at least 45 minutes and were probed with anti-Mfn1 antibody and anti-Mfn2 antibody for 4 hours at room temperature or overnight at 4°C. Membranes were incubated with DyLight secondary antibody (Invitrogen) at room temperature for 1 hour. Membranes were imaged on LI-COR Imaging System (LI-COR Biosciences).

Western Blot Analysis

Protein lysates from MEFs were obtained by resuspending PBS washed cells in RIPA lysis buffer (150 mM NaCl, 1% Nonidet P-40, 1% Sodium deoxycholate, 0.1% SDS, 25 mM Tris [pH 7.4], 1X Halt Protease Inhibitor Cocktail, EDTA-Free [Thermo Scientific]). Samples were incubated on ice for 5 minutes and then spun at 21,000 x g for 15 minutes at 4°C. Supernatant was transferred to a clean tube and protein concentration was measured by BCA assay (Thermo Scientific). Samples were run on an SDS-PAGE gel and transferred onto nitrocellulose at 100 V for 50 minutes in 1X transfer buffer. Membranes were blocked in 4% milk for at least 45 minutes and were probed with anti-Mfn1, anti-Mfn2 (Sigma), anti-VDAC (Invitrogen) or anti-alpha Tubulin (Invitrogen) antibody for 4 hours at room temperature or overnight at 4°C. Membranes were incubated with DyLight secondary antibody (Invitrogen) at room temperature for 1 hour. Membranes were imaged on LI-COR Imaging System (LI-COR Biosciences).

Plasmids & primers

The following plasmids were purchased from Addgene: pBABE-hygro (#1765), pBABE-puro (#1764), mito-PAGFP (#23348), pclbw-mito TagRFP (#58425), pclbw-mitoCFP (#58426). The following primers were used to for site directed mutagenesis by Gibson Assembly:

$Mfn2^{S378P}$ F: (5' – CCGTTCGTCTCATCATGGATCCCCTGCACATCGCAGC – 3')

$Mfn2^{S378P}$ R: (5' – GCTGCGATGTGCAGGGGATCCATGATGAGACGAACGG – 3')

$Mfn2^{A383V}$ F: (5' – ATTCCCTGCACATCGCAGTTCAGGAGCAGCGGG – 3')

$Mfn2^{A383V}$ R: (5' – CCCGCTGCTCCTGAACTGCGATGTGCAGGGAAT – 3')

$Mfn2^{Q386P}$ F: (5' –GCACATCGCAGCTCAGGAGCCGCGGGTTTATTGCCTAGAAATGCGG -3')

$Mfn2^{Q386P}$ R: (5'- CCGCATTTCTAGGCAATAAACCCGCGGCTCCTGAGCTGCGATGTGC -3')

$Mfn2^{C390F}$ F: (5' – GGGTTTATTTCCTAGAAATGCGG – 3')

$Mfn2^{C390F}$ R: (5' – CCGCATTTCTAGGAAATAAACCC – 3')

$Mfn2^{L710P}$ F: (5' – GACATCACCCGAGATAATCCGGAGCAGGAAATTGCTGC – 3')

$Mfn2^{L710P}$ R: (5' – GCAGCAATTTCCTGCTCCGGATTATCTCGGGTGATGTC – 3')

ACKNOWLEDGEMENTS

We thank the members of the Hoppins lab and Laura Lackner for critical scientific discussions and critical reading of the manuscript. NBS was supported by National Institute of General Medical Sciences (NIH NIGMS) Training grant No. T32GM007270 and SCH is supported by NIH NIGMS Grant No. R01GM-118509.

REFERENCES

Brandt, T. et al., 2016. A mitofusin-dependent docking ring complex triggers mitochondrial fusion in vitro. *eLife*, 5, pp.1–23.

Brockmann, K. et al., 2008. Cerebral involvement in axonal Charcot-Marie-Tooth neuropathy caused by mitofusin2 mutations. *Journal of Neurology*, 255(7), pp.1049–1058.

Cao, Y.-L. et al., 2017. MFN1 structures reveal nucleotide-triggered dimerization critical for mitochondrial fusion. *Nature*, pp.1–5.

Celardo, I., Martins, L.M. & Gandhi, S., 2014. Unravelling mitochondrial pathways to Parkinson's disease. *British Journal of Pharmacology*, 171(8), pp.1943–1957.

Chen, H. et al., 2003. Mitofusins Mfn1 and Mfn2 coordinately regulate mitochondrial fusion and are essential for embryonic development. *Journal of Cell Biology*, 160, pp.189–200.

Detmer, S. a. & Chan, D.C., 2007. Complementation between mouse Mfn1 and Mfn2 protects mitochondrial fusion defects caused by CMT2A disease mutations. *Journal of Cell Biology*, 176(4), pp.405–414.

Detmer, S.A. & Chan, D.C., 2007a. Complementation between mouse Mfn1 and Mfn2 protects mitochondrial fusion defects caused by CMT2A disease mutations. *The Journal of cell biology*, 176(4), pp.405–14.

Detmer, S.A. & Chan, D.C., 2007b. Functions and dysfunctions of mitochondrial dynamics. *Nature reviews. Molecular cell biology*, 8(november), pp.870–879.

Engelhart, E.A. & Hoppins, S., 2019. A catalytic domain variant of Mitofusin requiring a wildtype paralog for function uncouples mitochondrial outer-membrane tethering and fusion. *Journal of Biological Chemistry*, 1(8), p.jbc.RA118.006347.

Eura, Y., 2003. Two Mitofusin Proteins, Mammalian Homologues of FZO, with Distinct Functions Are Both Required for Mitochondrial Fusion. *Journal of Biochemistry*, 134(3), pp.333–344.

Feely, S.M.E. et al., 2011. MFN2 mutations cause severe phenotypes in most patients with CMT2A. *Neurology*, 76(20), pp.1690–6.

Franco, A. et al., 2016. Correcting mitochondrial fusion by manipulating mitofusin conformations. *Nature*, pp.1–20.

Gemignani, F. & Marbini, A., 2001. Charcot-Marie-Tooth disease (CMT): Distinctive phenotypic

and genotypic features in CMT type 2. *Journal of the Neurological Sciences*, 184(1), pp.1–9.

Griffin, E.E. & Chan, D.C., 2006. Domain interactions within Fzo1 oligomers are essential for mitochondrial fusion. *The Journal of biological chemistry*, 281(24), pp.16599–606.

Hoppins, S. et al., 2011. The Soluble Form of Bax Regulates Mitochondrial Fusion via MFN2 Homotypic Complexes. *Molecular Cell*, 41(2), pp.150–160.

Horbay, R. & Bilyy, R., 2016. Mitochondrial dynamics during cell cycling. *Apoptosis*, 21(12), pp.1327–1335.

Ishihara, N., 2004. Mitofusin 1 and 2 play distinct roles in mitochondrial fusion reactions via GTPase activity. *Journal of Cell Science*, 117(26), pp.6535–6546.

Jimah, J.R. & Hinshaw, J.E., 2019. Structural Insights into the Mechanism of Dynamin Superfamily Proteins. *Trends in Cell Biology*, 29(3), pp.257–273.

Koshiba, T. et al., 2004. Structural basis of mitochondrial tethering by mitofusin complexes. *Science (New York, N.Y.)*, 305(5685), pp.858–862.

Labbé, K., Murley, A. & Nunnari, J., 2014. Determinants and Functions of Mitochondrial Behavior. *Annual Review of Cell and Developmental Biology*, 30(1), pp.357–391.

Low, H.H. et al., 2009. Structure of a Bacterial Dynamin-like Protein Lipid Tube Provides a Mechanism For Assembly and Membrane Curving. *Cell*, 139(7), pp.1342–1352.

Low, H.H. & Löwe, J., 2006. A bacterial dynamin-like protein. *Nature*, 444(7120), pp.766–769.

Muglia, M. et al., 2009. A novel founder mutation in the MFN2 gene associated with variable Charcot-Marie-Tooth type 2 phenotype in two families from Southern Italy. *BMJ Case Reports*, pp.1–2.

Qi, Y. et al., 2016. Structures of human mitofusin 1 provide insight into mitochondrial tethering.

Rocha, A.G. et al., 2018. MFN2 agonists reverse mitochondrial defects in preclinical models of Charcot-Marie-Tooth disease type 2A. *Science*, 360(6386), pp.336–341.

Rovira-Llopis, S. et al., 2017. Mitochondrial dynamics in type 2 diabetes: Pathophysiological implications. *Redox Biology*, 11(January), pp.637–645.

Santel, a & Fuller, M.T., 2001. Control of mitochondrial morphology by a human mitofusin. *Journal of cell science*, 114, pp.867–874.

Scorrano, L., 2013. Keeping mitochondria in shape: A matter of life and death. *European Journal of Clinical Investigation*, 43(8), pp.886–893.

Stuppia, G. et al., 2015. MFN2-related neuropathies: Clinical features, molecular pathogenesis and therapeutic perspectives. *Journal of the Neurological Sciences*.

Tondera, D. et al., 2009. SLP-2 is required for stress-induced mitochondrial hyperfusion. *The EMBO journal*, 28(November 2008), pp.1589–1600.

Verhoeven, K. et al., 2006. MFN2 mutation distribution and genotype/phenotype correlation in Charcot-Marie-Tooth type 2. *Brain*, 129(8), pp.2093–2102.

Vital, A. & Vital, C., 2012. Mitochondria and peripheral neuropathies. *Journal of neuropathology and experimental neurology*, 71(12), pp.1036–46.

Wada, J. & Nakatsuka, A., 2016. Mitochondrial Dynamics and Mitochondrial Dysfunction in Diabetes. *Acta medica Okayama*, 70(3), pp.151–8.

Yan, L. et al., 2018. Structural basis for GTP hydrolysis and conformational change of MFN1 in mediating membrane fusion. *Nature Structural and Molecular Biology*, 25(3), pp.233–243.

Yang, J. & Zhang, Y., 2015. I-TASSER server: New development for protein structure and function predictions. *Nucleic Acids Research*, 43(W1), pp.W174–W181.

Zhang, Y., 2009. I-TASSER: Fully automated protein structure prediction in CASP8. *Proteins: Structure, Function and Bioinformatics*, 77(SUPPL. 9), pp.100–113.

Zhou, Y. et al., 2019. Restoring mitofusin balance prevents axonal degeneration in a Charcot-Marie-Tooth type 2A model Graphical abstract Find the latest version : Restoring mitofusin balance prevents axonal degeneration in a Charcot-Marie-Tooth type 2A model.

Züchner, S. et al., 2004. Mutations in the mitochondrial GTPase mitofusin 2 cause Charcot-Marie-Tooth neuropathy type 2A. *Nature genetics*, 36(5), pp.449–451.